ARTICLES
PUBLISHED ONLINE: 3 AUGUST 2015 | DOI: 10.1038/NNANO.2015.160
nature nanotechnology

High-frequency nano-optomechanical disk resonators in liquids

E. Gil-Santos[1], C. Baker[1], D. T. Nguyen[1], W. Hease[1], C. Gomez[2], A. Lemaître[2], S. Ducci[1], G. Leo[1] and I. Favero[1]*

Nano- and micromechanical resonators are the subject of research that aims to develop ultrasensitive mass sensors for spectrometry, chemical analysis and biomedical diagnosis. Unfortunately, their merits generally diminish in liquids because of an increased dissipation. The development of faster and lighter miniaturized devices would enable improved performances, provided the dissipation was controlled and novel techniques were available to drive and readout their minute displacement. Here we report a nano-optomechanical approach to this problem using miniature semiconductor disks. These devices combine a mechanical motion at high frequencies (gigahertz and above) with an ultralow mass (picograms) and a moderate dissipation in liquids. We show that high-sensitivity optical measurements allow their Brownian vibrations to be resolved directly, even in the most-dissipative liquids. We investigate their interaction with liquids of arbitrary properties, and analyse measurements in light of new models. Nano-optomechanical disks emerge as probes of rheological information of unprecedented sensitivity and speed, which opens up applications in sensing and fundamental science.

The development of ultrasensitive mechanical sensors for biological applications, such as early disease detection, has recently generated a great deal of effort[1–4]. In this context, mass sensors based on micro- and nanomechanical resonators appear as a key technology, as exemplified by their capability to sense down to individual atoms in a vacuum[5–7]. In short, the minimum detectable mass is proportional to the effective mass of the resonator, and the sensitivity improves when the mechanical dissipation is reduced. Both device miniaturization and dissipation control are therefore crucial. In the liquid environments typically required for biological applications, most mechanical resonators suffer from high energy losses that dramatically diminish the mass sensitivity[8,9]. Furthermore, viscous damping in a liquid also increases when standard mechanical devices, such as cantilevers or membranes, are miniaturized[10].

To circumvent these problems novel structures and techniques have been developed. An efficient approach is to use vibrating microchannel cantilevers in which the liquid flows directly inside the resonator to reduce the induced dissipation[11–13]. Fibred microcapillaries[14,15] adopt this approach too and combine it with guided optics to obtain an efficient optical detection that takes place in a capillary bubble. As both types of device need to embed fluidic channels, their size varies from a few tens to a few hundreds of microns, which leads to masses greater than the nanogram level and fundamental mechanical frequencies in the megahertz range at most. These channel devices are difficult to miniaturize to the nanoscale. Other approaches investigated include the cases of partially immersed[16] and feedback laser-controlled[17] resonators, but these also face size limitations and have demonstrated poorer integration capabilities.

Here we highlight the potential of a nano-optomechanical approach in this context, with a particular focus on miniature (subcubic-micrometre volume) semiconductor disk resonators and their (contour) mechanical radial breathing modes (RBMs). These resonators can be completely immersed in a liquid, which allows an *in situ* fluidic operation, and they provide reduced dimensions compatible with multiple sites on a single chip and a high throughput. Although their low inertial mass (picograms), high mechanical frequencies beyond gigahertz values and moderate fluidic dissipation are clear assets for sensing applications, so far they have not been investigated in liquids[18,19]. Indeed, the typical mechanical displacement associated with RBMs is extremely small and difficult to detect with conventional techniques, especially in a liquid and at very high frequencies. Here we show that nano-optomechanics[20,21] provides the required bandwidth and precision to meet this experimental challenge. Miniature disks support optical whispery gallery modes (WGMs) with a high optical quality factor ($Q > 10^5$) that strongly couple to RBMs[22,23] to yield a displacement sensitivity of 10^{-17} m $Hz^{-1/2}$ (ref. 18). Exploiting these features, we are able to resolve optomechanically the Brownian motion of disk resonators at gigahertz frequencies, even in the most-dissipative liquids. The technique enables us to study in great detail the fluid–structure interaction. We interpret our experimental results with new analytical models that directly reveal the influence of various physical parameters involved in viscous and acoustic interactions. These models lead us to quantify the unprecedented sensitivity of nano-optomechanical disk resonators to mass deposition and other rheological changes in liquids, which sets the stage for a variety of sensing and basic science applications at very high frequency.

In this work, miniature disk resonators and their pedestal are fabricated out of gallium arsenide (GaAs) and aluminium gallium arsenide (AlGaAs), whose epitaxial control provides a low-dissipation high-purity crystal and the possibility of engineering optomechanical heterostructures[24,25]. However, the general implications of our work also extend to other mature semiconductor platforms with similar refractive properties, such as silicon. In our experiments, the disk thickness is kept constant (320 nm), whereas the disk radius is varied from 1 to 3 μm. Monochromatic

[1]Matériaux et Phénomènes Quantiques, Université Paris Diderot, CNRS, Sorbonne Paris Cité, UMR 7162, 10 rue Alice Domon et Léonie Duquet, Paris 75013, France. [2]Laboratoire de Photonique et Nanostructures, CNRS, Route de Nozay, Marcoussis 91460, France. *e-mail: ivan.favero@univ-paris-diderot.fr

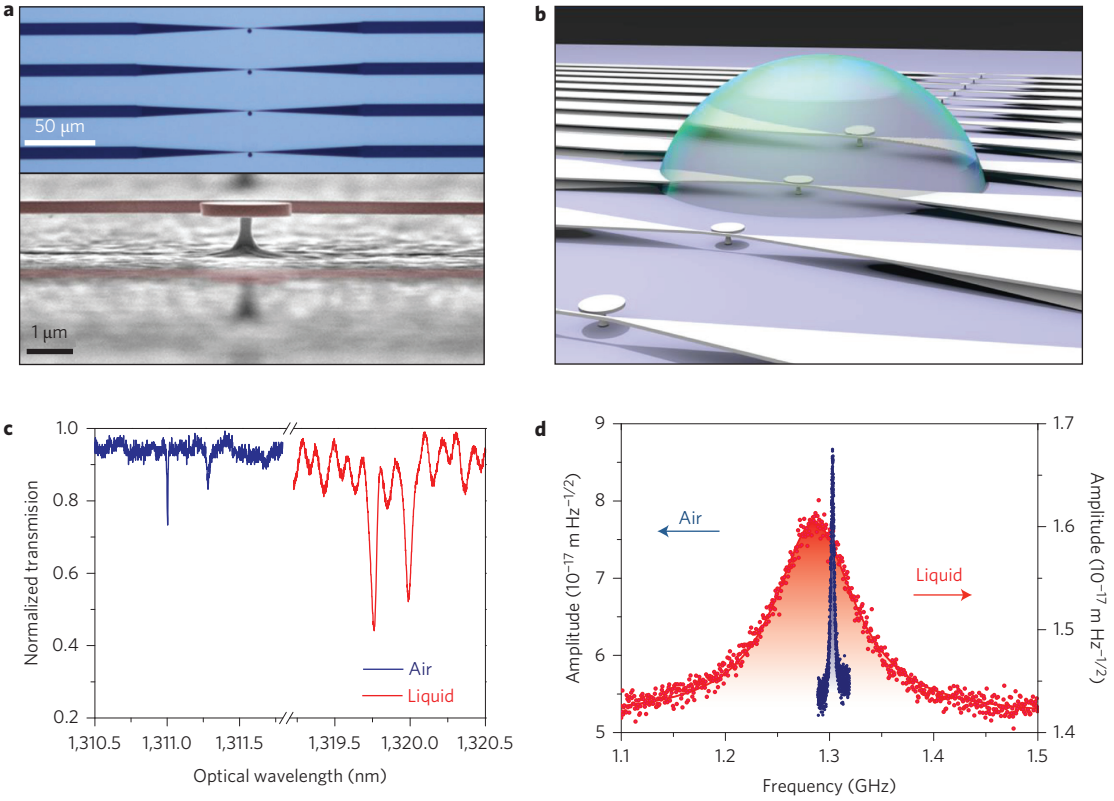

Figure 1 | Operation of nano-optomechanical disks in a liquid. a, Upper panel: optical microscope top view of four tapered waveguides and disk resonators[26]. Lower panel: scanning electron microscope side view of a GaAs disk resonator on its AlGaAs pedestal in front of the suspended tapered part of the optical waveguide. **b**, Schematic representation of resonators immersed in a liquid droplet. **c**, Optical transmission spectra of a 1 μm radius disk in air (dark blue) and in liquid (red). **d**, Thermomechanical spectra of the disk vibrating in air (dark blue) and in liquid (red) acquired by optomechanical measurement.

light at $\lambda = 1.3$ μm is evanescently coupled into the disk through a GaAs-tapered waveguide fabricated on a chip in the disk's vicinity[26]. A typical chip is 1 mm long, 3 mm wide and contains 100 waveguides/disk units separated by a 30 μm gap distance (see Fig. 1a). Much denser chips can be obtained with the same fabrication process. Thanks to the large refractive index of GaAs, the disk/waveguide structures can be immersed in a transparent liquid and still preserve their light-guiding properties, that is, leave their overall optical transmittance unaffected. A microlitre droplet of liquid, deposited on the sample surface with a micropipette (see Fig. 1b), covers many resonators and lasts from a few minutes to hundreds of minutes before evaporating. After immersion, the disk WGM resonances are redshifted and slightly broadened, as apparent in Fig. 1c. These effects result from the refractive action of the surrounding liquid, as confirmed by finite element method (FEM) simulations (see the Supplementary Information). For a radius of 1 μm, Fig. 1c reports a loaded optical Q of 2.2×10^4 in the liquid. Owing to the subcubic-micrometre volume of their photon–phonon interaction, miniature disks yield an intense optomechanical coupling. The coupling strength is standardly parameterized by the shift g_0 of the optical cavity resonance produced by a mechanical displacement that amounts to the amplitude of the zero-point fluctuations[21]. It attains $g_0 = 2$ MHz (refs 22,23) in the present work, a value that combines with the high optical Q to lead to a motional sensitivity down to 10^{-17} m Hz$^{-1/2}$. In our experiments, the optomechanical coupling allows an efficient transduction of the mechanical motion, but does not lead to its modification through back-action effects. The achieved sensitivity is sufficient to resolve the minute thermal (Brownian) fluctuations of the mechanical system, even in a liquid. Figure 1d shows mechanical spectra obtained by such optomechanical measurements in the Brownian motion regime before and after immersion. Here again, the effect of immersion is twofold: a redshift of the mechanical frequency that resembles an added motional inertia, and a broadening of the resonance that corresponds to the added dissipation. We now provide an in-depth analysis of the dispersive and dissipative facets of the fluid–structure interaction.

The mechanical behaviour of a GaAs disk in a fluid is expected to depend both on the disk dimensions and the fluid properties, which motivated the measurement of resonators of different radii immersed in different liquids. Figure 2 reports the measured mechanical Q_m and relative mechanical frequency shift $\Delta f/f$ of disks with radii that vary from 1 to 3 μm immersed in three significantly distinct liquids of which the dynamic viscosity μ, density ρ and speed of sound c are listed in Table 1. These measurements were carried out in the low optical power limit, as discussed in the Supplementary Information. Although our goal below is to interpret these results, we emphasize first that the general problem of a mechanical element interacting with an arbitrary liquid is extremely complex, as it formally merges elasticity theory and generalized Navier–Stokes equations. Exact solutions are certainly out of reach, but some considerations are possible in simplified hydrodynamic situations. In the incompressible viscous-liquid case, the disk motion dissipates energy through fluidic friction in proportion to the viscosity parameter μ (viscous regime). Added motional inertia occurs as well, induced by the displaced mass of liquid, in proportion to ρ. In the frictionless compressible-liquid case (acoustic regime), the moving disk generates outgoing pressure waves in the liquid, which leads to dissipation and a modified vibration

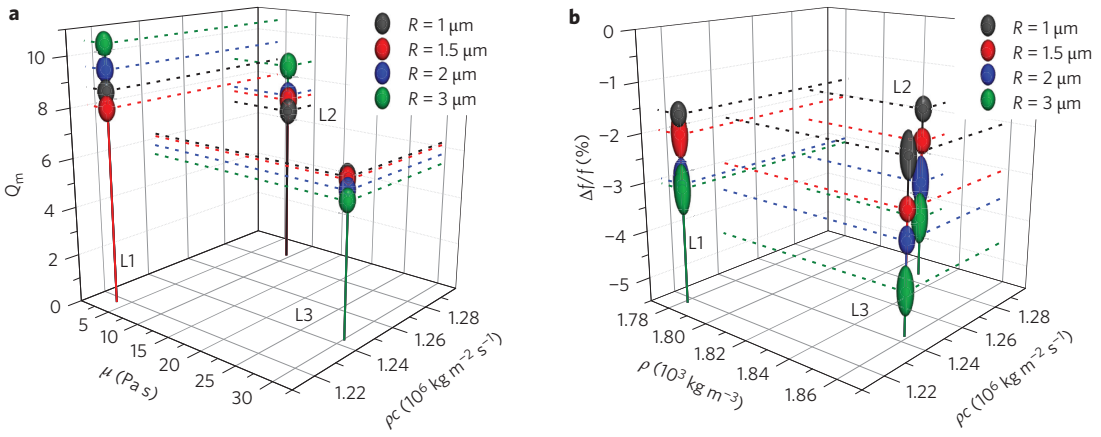

Figure 2 | Dissipative and dispersive fluid-structure interactions measured by nano-optomechanical means. a, Mechanical quality factor Q_m measured for four distinct disk radii in three distinct liquids plotted versus the viscosity and acoustic impedance of the liquid. **b**, Relative mechanical shift $\Delta f/f$ for the same set of measurements plotted versus the density and the acoustic impedance of the liquid. The symbol vertical size corresponds to the s.d.

frequency. To grasp these different aspects of the fluid–structure interaction, Fig. 2 shows a plot of the measured Q_m as a function of viscosity and acoustic impedance (ρc) of the liquid, and one of $\Delta f/f$ versus density and acoustic impedance. Under such a representation, some trends appear in the measurements. First, whatever the size of the disk, Q_m decreases as μ increases, as expected from viscous interactions. Second, the negative magnitude of $\Delta f/f$ increases as ρ increases, as anticipated from an added-mass picture. The behaviour as a function of the acoustic impedance is less obvious. Q_m and $\Delta f/f$ are non-monotonous functions of ρc, which suggests the impedance-matching conditions elucidated below. From the magnitude of these effects, our measurements indicate that both viscous and acoustic interactions must be taken into account to describe accurately the behaviour of nano-optomechanical resonators operated in liquids. This stands in contrast to mechanical systems of lower frequency, which tend to dwell in the viscous regime for common fluids, such as water or air[10,27]. Both numerical and new analytical models of viscous and acoustic interactions are proposed below and are utilized to interpret the experimental results. Analytical expressions lead us to reveal directly the unusual potential of nano-optomechanical disks as sensors of mass deposition and other rheological changes in liquids.

A key feature of optomechanical disks vibrating on their RBM is that they possess rotational invariance around their vertical axis, provided their constitutive elastic material is considered isotropic. In an isotropic liquid, this symmetry enables us to reduce the difficult three-dimensional (3D) fluid–structure interaction problem to a more tractable 2D one. The FEM then allows us to perform reliable numerical calculations of the disk vibrating in the liquid, both in the incompressible viscous regime and in the purely acoustic regime. Details of these FEM calculations, which provide a first-analysis tool for the present work, are given in the Supplementary Information.

The rotational symmetry has other consequences as well. For a small-radius pedestal, the RBM of the disk can be approximated by the radial contour mode of a free circular elastic plate, which can be computed analytically[22,28,29]. By means of the Poisson effect, this radial extensional mode is accompanied by compression and extension ('pinching') of the disk's thickness, which can also be described analytically with high precision (see the Supplementary Information). We build on this analytical description of the RBM to develop an analytical theory of the fluid–disk interaction, adapting the hydrodynamic formula valid for a sphere[27,30]. Indeed, as a result of its perfect symmetry, the sphere with its centre of mass vibrating harmonically along one direction in a viscoelastic liquid is a problem that admits an exact solution, which was derived by Oestreicher[31]. In this derivation, the complete velocity field in the fluid was solved, which allows us to express the fluidic force exerted on any point of the sphere surface. In the disk case, we sum these fluidic forces over the vibrational profile of the structure to account precisely for the response of the liquid against the radial and the out-of-plane 'pinching' motion (see the Supplementary Information). This approach allows us to encompass dissipative and dispersive fluid–structure interactions with a very satisfactory precision.

First, we analyse the incompressible viscous regime of the liquid. In this case, Oestreicher's formulae for the viscous force are integrated on our analytical profile of the RBM and lead to expressions (1) and (2) for the mechanical quality factor and the relative resonance frequency shift of the disk in the liquid (see the Supplementary Information):

$$Q_{\text{viscous}} = \frac{\rho_s \omega H R}{8.36\mu + (3.18H + R)\sqrt{2\rho\omega\mu}} \quad (1)$$

$$\left(\frac{\Delta f}{f}\right)_{\text{viscous}} = -\frac{1.27H}{2R}\frac{\rho}{\rho_s} - \frac{3.18/R + 1/H}{2\rho_s}\sqrt{2\rho\mu/\omega} \quad (2)$$

where R, H and ρ_s are the radius, thickness and density of the disk material, respectively. In these formulae, we see that dissipation not only stems from the fluid viscosity μ, but also from the dynamical term $\sqrt{\rho\omega\mu}$, which is actually dominant in the frequency regime of nano-optomechanical disks. Given the angular frequency expression for the first-order RBM of a circular plate[22], $\omega = (\lambda/R)\sqrt{E/\rho_s(1-\nu^2)}$ (with E and ν the Young modulus and Poisson ratio of the material, respectively), where the frequency parameter λ only depends on ν, we obtain the following scaling law from equation (1): $Q_{\text{viscous}} \propto (H\sqrt{R})/(3.18H + R)$. Accordingly, Q has a maximum at $R = 3.18H$ and increases with resonator size.

Table 1 | Properties of the liquids.

	ρ (kg m^{-3})	μ (mPa s)	c (m s^{-1})
Water	1,000	1	1,500
Liquid 1	1,782	3.5	669
Liquid 2	1,831	9	702
Liquid 3	1,859	30	683

The density, dynamic viscosity and speed of sound of water and the studied liquids are quoted at room temperature. Liquids 1, 2 and 3 are perfluorinated liquids of increasing viscosity and density.

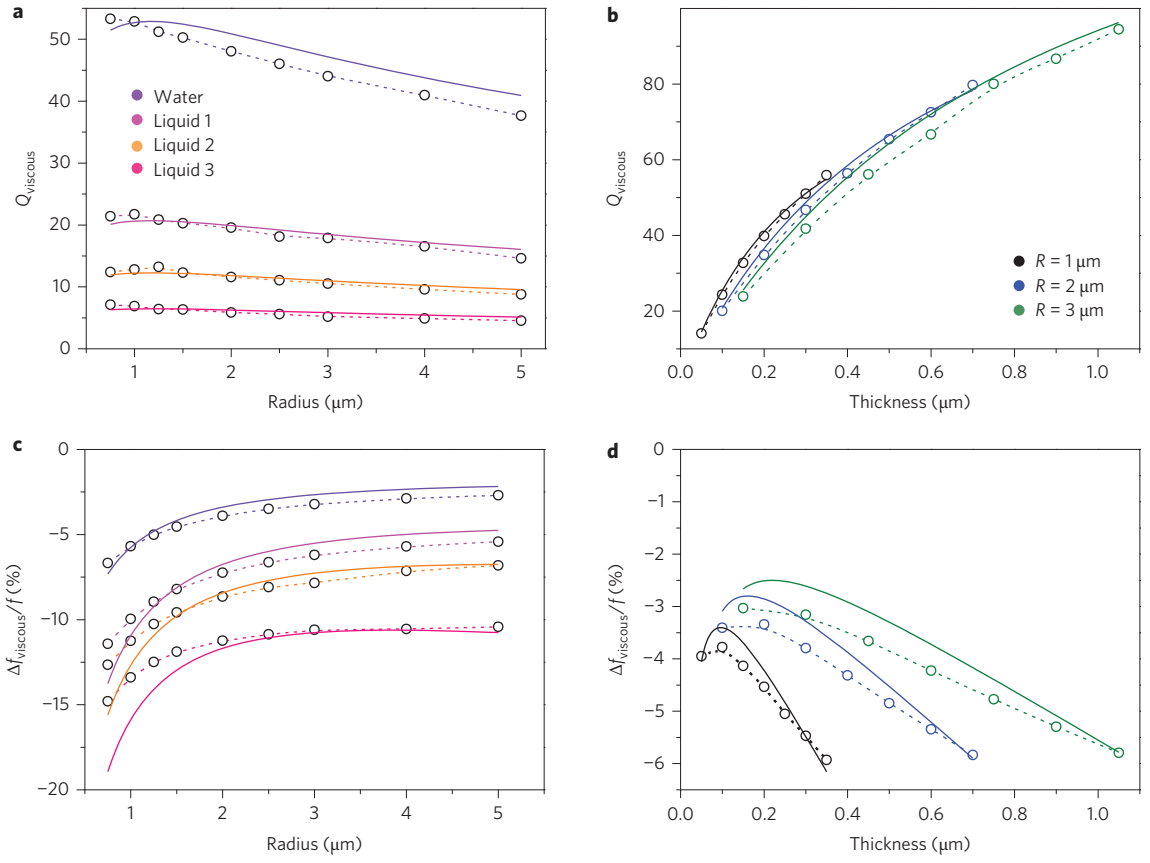

Figure 3 | Viscous regime models. Our analytical model (solid lines) is systematically compared with the FEM results (open circles with dashed lines). **a**, Mechanical quality factor versus disk radius for a fixed thickness of 320 nm in four distinct liquids. **b**, Mechanical quality factor versus disk thickness for three distinct radii when immersed in water. **c**,**d**, The corresponding relative mechanical frequency shift $\Delta f/f$ as a function of the same parameters.

Importantly, Q only diminishes by a factor of ten when H and R are reduced by a factor 100, which results in a reduction by a factor of 10^6 in the device mass. In this view, miniaturization of disks vibrating on their RBM appears appealing for Q-dependent applications in a viscous liquid, in contrast to standard cantilever devices[10]. On the dispersive side of the fluid–structure interaction, the mechanical frequency shift is proportional to the fluid density, but also to the dynamical term $\sqrt{\rho\mu/\omega}$, both of which have commensurable contributions for our miniature disks.

In Fig. 3 our analytical formulae are compared with numerical FEM simulations for the four different liquids considered in this work. For all the liquids, both the dissipative and dispersive parts of the fluid–structure interaction are reproduced as a function of the disk radius and thickness with a very satisfactory level of agreement. The Q maximum close to $R = 3.18H$ is, for example, directly visible in the FEM results. An excellent agreement as a function of the liquid's viscosity and density is also illustrated in the Supplementary Information.

We now analyse the acoustic regime. Following the same method as above, the fluidic force is integrated over the disk's surface to obtain the mechanical Q and relative frequency shift of the RBM in the fluid. Although this analytical approach reproduces qualitatively many aspects observed in FEM simulations, in the acoustic regime it fails in a more quantitative fit. This problem stems from interferences of compression waves emitted by the disk in the liquid, whose detailed patterns are not retrieved correctly by the analytical approach above. Still, the obtained analytical expressions are an excellent starting point to develop more-accurate empirical formulae. Guided by these analytical expressions and by the FEM calculations, we finally obtain the empirical formulae (3) and (4) (see the Supplementary Information):

$$Q^{-1}_{\text{acoustic}} = \frac{H}{R}\frac{\rho}{\rho_s}\left[1.92\frac{((1/2)(\lambda/\sqrt{1-\nu^2})(c_s/c))^3}{4+((1/2)(\lambda/\sqrt{1-\nu^2})(c_s/c))^4} + 1.05\left(\frac{H}{R}\right)^{-1/2}\frac{((3/4)(\lambda/\sqrt{1-\nu^2})(c_s/c)(H/R))^3}{4+((3/4)(\lambda/\sqrt{1-\nu^2})(c_s/c)(H/R))^4}\right] = f\left(\frac{H}{R},\frac{\rho}{\rho_s},\frac{c_s}{c},\nu\right) \quad (3)$$

$$\left(\frac{\Delta f}{f}\right)_{\text{acoustic}} = -0.954\frac{H}{R}\frac{\rho}{\rho_s}\left[\frac{1}{4+((1/4)(\lambda/\sqrt{1-\nu^2})(c_s/c))^4} + \frac{2.4}{4+((3/5)(\lambda/\sqrt{1-\nu^2})(c_s/c)(H/R))^4}\right] = g\left(\frac{H}{R},\frac{\rho}{\rho_s},\frac{c_s}{c},\nu\right) \quad (4)$$

Importantly, expressions (3) and (4) can be cast into simple functions of the dimensionless parameters H/R, ρ/ρ_s, c/c_s and ν. Regarding dissipation, the dependence of Q on the geometric factor H/R shows that the disk mass can be miniaturized at constant H/R while maintaining constant Q, which again leads to improved performances with miniaturized devices. A second lesson brought by these formulae is that the density and speed-of-sound ratios

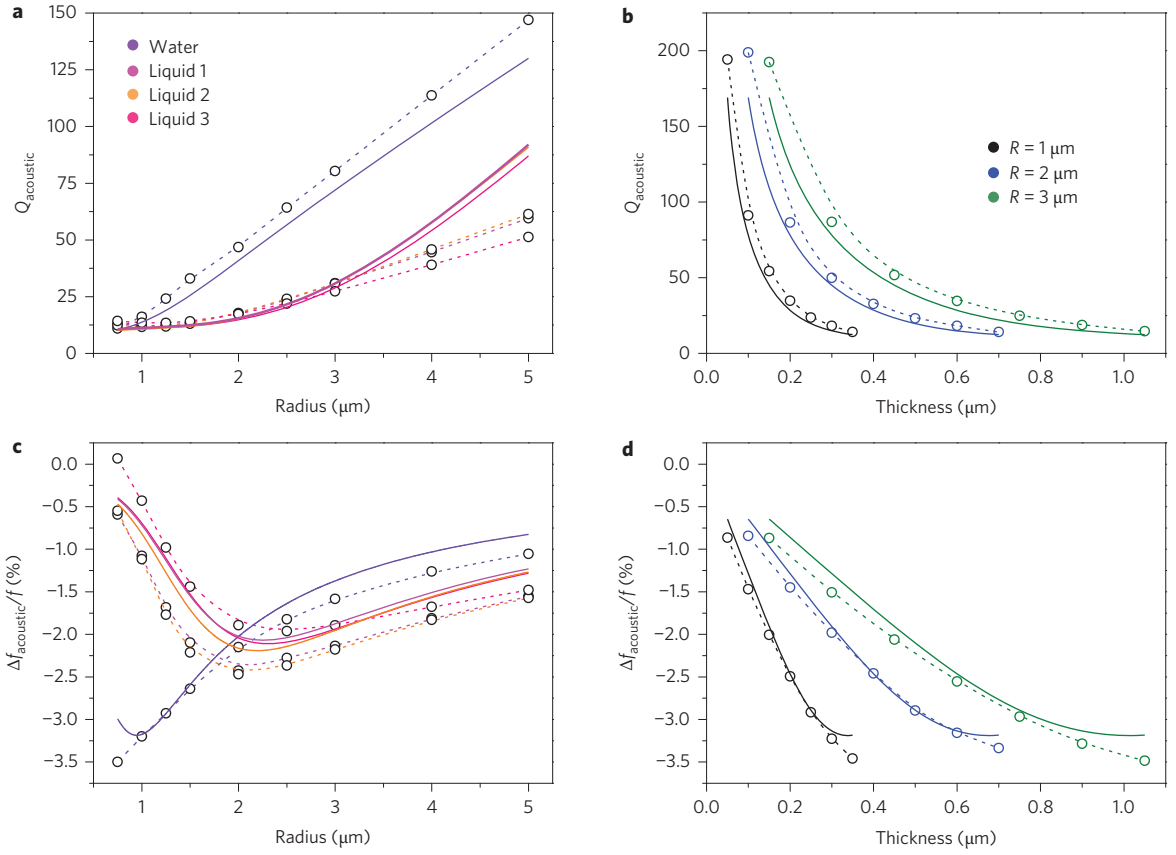

Figure 4 | Acoustic regime models. Our analytical model (solid lines) is systematically compared with the FEM results (open circles with dashed lines). **a**,**b**, Mechanical quality factor versus the disk radius for a fixed thickness of 320 nm in the same four distinct liquids as in Fig. 3 (**a**), and versus the disk thickness for three distinct radii when immersed in water (**b**). **c**,**d**, The corresponding relative mechanical shift $\Delta f/f$ as a function of the same parameters.

(ρ/ρ_s and c/c_s, respectively) each play a separate role, in contrast to the standard case of acoustic plane-wave propagation that only involves the acoustic impedance ratio $\rho c/\rho_s c_s$. As far as the mechanical shift is concerned, the linear dependence with ρ supports the picture of an added mass by the liquid. Also, we retrieve the scaling relation $\Delta f/f \propto H\rho/R\rho_s$, which was already present in the first term of the corresponding viscous expression.

These analytical acoustic-regime formulae are compared with numerical FEM simulations in Fig. 4 for the four liquids. For all the liquids, the evolution of Q and $\Delta f/f$ as a function of disk radius and thickness is reproduced satisfactorily, with quantitative discrepancies typically limited to below 20%. A convincing agreement is also demonstrated (see the Supplementary Information) as a function of the liquid's density and speed of sound.

With these new models in hand, we now interpret our experimental results. Figure 5a reports the mechanical Q of disks with radii that vary between 1 and 3 μm, measured in liquids 1, 2 and 3. The measurements are satisfactorily reproduced by both our FEM (dashed lines) and analytical models (not shown to avoid redundancy) when summing the dissipation associated with viscous and acoustic interactions. As the fluidic parameters viscosity, density and speed of sound are known independently for each liquid, there is no free parameter left in this agreement. The model predicts a Q that reaches 30 in water for a radius of 4 μm. At 1 μm, the acoustic dissipation dominates and sets $Q = 12$, which leads to a remarkable Q-frequency product, Qf, of 1.8×10^{10} in water. The minimum detectable mass can be evaluated using the well-established formula[32,33]

$$\delta m_{min} = 2m\sqrt{(B/2\pi Qf)\,(k_B T/E_{max})}$$

where m is the effective motional mass of the device, B the measurement bandwidth and E_{max} the maximal mechanical energy stored in the resonator. For contour modes, E_{max} is limited by the intrinsic mechanical nonlinearity of the material[34,35]. In silicon, the nonlinearity settles at an energy density, E_{max}/V, of 2×10^5 J m^{-3} for a bulk acoustic wave resonator with $Q > 10^5$, which extrapolates to 2×10^9 J m^{-3} for the present $Q = 12$, a value that should not differ much in GaAs[36]. With these parameters, the minimum mass detectable for an integration time of one second is 14 yg. Mass detection at this level has been demonstrated only in experiments that employ carbon nanotubes at cryogenic temperature under vacuum[7]. Although recent vibrating-channel devices in water approached the 10 zg range[37], the yoctogram regime remains unexplored in liquids. To explore further the potential of nano-optomechanical disks as sensors of fluidic information, we focus in Fig. 5b on the mechanical shifts measured in liquid 1. This is the least viscous of the three perfluorinated liquids, such that the acoustic model alone (solid line) suffices to explain the experimental results. Hence, equation (4) is employed to evaluate the sensitivity of the device to density changes in moderately viscous liquids like water. For the same disk as above placed in water, equation (4) leads to an approximate scaling with density $\Delta f \propto \rho$, with little role played by changes in the speed of sound. The thermodynamic limit of detection of density changes amounts, then, to $\delta\rho_{min} = 2 \times 10^{-7}$ kg m^{-3} for one second of integration time. This 10^{-10} relative sensitivity represents an improvement of three orders of magnitude over established techniques such as magnetic densimeters[38]. Finally, Fig. 5c focuses on the most-viscous liquid. At high viscosity, the assumption that viscous and acoustic losses are independent breaks down and experimental results are better explained by the

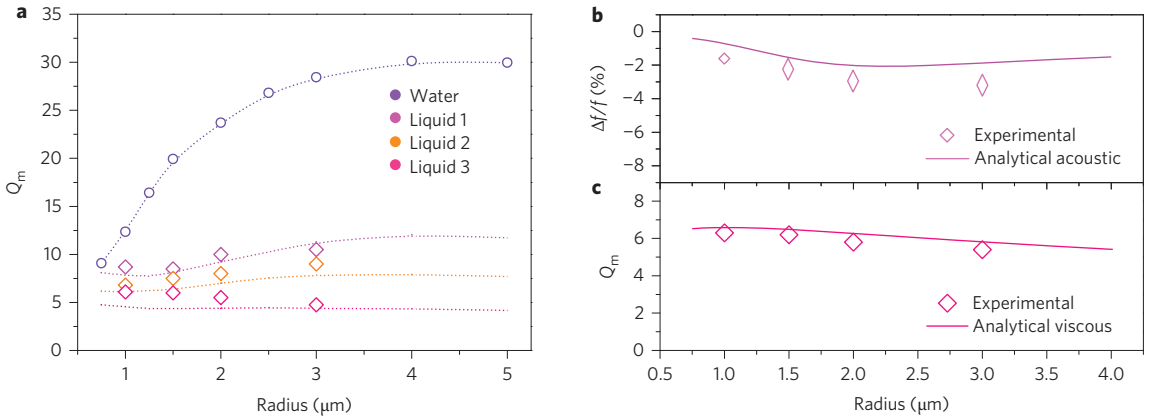

Figure 5 | Interpretation of nano-optomechanical experiments in liquids. a, Radius-dependent mechanical quality factor measured in liquids (open diamond symbols) and the fit obtained by summing the viscous and acoustic dissipations calculated by FEM (dashed lines). A convincing agreement is observed over the whole range of parameters. The most-precise fit is obtained for the least-viscous water-like liquids. The FEM results for water are shown in open violet circles linked by a dashed line. **b**, Radius-dependent mechanical shifts measured in liquid 1 and fitted by the analytical acoustic model. **c**, Radius-dependent mechanical quality factor measured in liquid 3 and fitted by the analytical viscous model.

viscous model alone (solid line). The validity of the analytical formulae in the most-viscous liquids again allows us to evaluate the sensitivity to viscosity changes, which leads to a relative sensitivity of $(\delta\mu/\mu)_{\min} = 5 \times 10^{-12}$ for the same disk as above. These ultimate mass and rheological sensitivities, quoted at the thermodynamic limit, clearly show the potential of scaling down microfabricated optomechanical resonators to the nanoscale. The smallest disks experimented with here reach a mechanical and optical subcubic-micrometre mode volume, but further miniaturization may lead to performances that are even-more stunning.

In this work, optomechanical techniques allow us to resolve the Brownian motion of nanoscale resonators in liquids, which paves the way to the low-noise optical driving of gigahertz motion through radiation pressure and electrostriction. We used the precision of nano-optomechanical techniques to validate original hydrodynamic models at a very high frequency. Not only does this give miniature-disk fluidic sensors a firm footing, but it also provides a reliable picture of nano-optomechanical dissipation in liquids. This is of importance for applications to come, ranging from quantum-enhanced technologies in aqueous environments[39] to high-speed optomechanical imaging probes. The concept of nano-optomechanical disks in liquids opens several routes that will all benefit from the mature technological control of semiconductors, which offers optoelectronic integration, lab-on-chip protocols and massively parallel architectures.

Methods

Methods and any associated references are available in the online version of the paper.

Received 20 February 2015; accepted 22 June 2015; published online 3 August 2015

References

1. Waggoner, P. S. & Craighead, H. G. Micro- and nanomechanical sensors for environmental, chemical, and biological detection. *Lab Chip* **7,** 1238–1255 (2007).
2. Arlett, J. L., Myers, E. B. & Roukes, M. L. Comparative advantages of mechanical biosensors. *Nature Nanotech.* **6,** 203–215 (2011).
3. Tamayo, J., Kosaka, P. M., Ruz, J. J., San Paulo, A. & Calleja, M. Biosensors based on nanomechanical systems. *Chem. Soc. Rev.* **42,** 1287–1311 (2013).
4. Ramos, D., Tamayo, J., Mertens, J., Zaballos, A. & Calleja, M. Origin of the response of nanomechanical resonators to bacteria adsorption. *J. Appl. Phys.* **100,** 106105 (2006).
5. Hanay, M. S. *et al.* Single-protein nanomechanical mass spectrometry in real time. *Nature Nanotech.* **7,** 602–608 (2012).
6. Naik, A. K., Hanay, M. S., Hiebert, W. K., Feng, X. L. & Roukes, M. L. Towards single-molecule nanomechanical mass spectrometry. *Nature Nanotech.* **4,** 445–450 (2009).
7. Chaste, J. *et al.* A nanomechanical mass sensor with yoctogram resolution. *Nature Nanotech.* **7,** 300–303 (2012).
8. Ekinci, K. L. & Roukes, M. L. Nanoelectromechanical systems. *Rev. Sci. Instrum.* **76,** 061101 (2005).
9. Eom, K., Park, H. S., Yoon, D. S. & Kwon, T. Nanomechanical resonators and their applications in biological/chemical detection: nanomechanics principles. *Phys. Rep.* **503,** 115–163 (2011).
10. Sader, J. E. Frequency response of cantilever beams immersed in viscous fluids with applications to the atomic force microscope. *J. Appl. Phys.* **84,** 64–76 (1998).
11. Lee, J., Shen, W., Payer, K., Burg, T. P. & Manalis, S. R. Toward attogram mass measurements in solution with suspended nanochannel resonators. *Nano Lett.* **10,** 2537–2542 (2010).
12. Burg, T. P. *et al.* Weighing of biomolecules, single cells and single nanoparticles in fluid. *Nature* **446,** 1066–1069 (2007).
13. Agache, V., Blanco-Gomez, G., Baleras, F. & Caillat, P. An embedded microchannel in a MEMS plate resonator for ultrasensitive mass sensing in liquid. *Lab Chip* **11,** 2598–2603 (2011).
14. Bahl, G. *et al.* Brillouin cavity optomechanics with microfluidic devices. *Nature Commun.* **4,** 1994 (2013).
15. Kim, K. H. *et al.* Cavity optomechanics on a microfluidic resonator with water and viscous liquids. *Light Sci. Appl.* **2,** e110 (2013).
16. Linden, J., Thyssen, A. & Oesterschulze, E. Suspended plate microresonators with high quality factor for the operation in liquids. *Appl. Phys. Lett.* **104,** 191906 (2014).
17. Ramos, D., Mertens, J., Calleja, M. & Tamayo, J. Photothermal self-excitation of nanomechanical resonators in liquids. *Appl. Phys. Lett.* **92,** 173108 (2008).
18. Ding, L. *et al.* High frequency GaAs nano-optomechanical disk resonator. *Phys. Rev. Lett.* **105,** 263903 (2010).
19. Clark, J. R., Hsu, W. T., Abdelmoneum, M. A. & Nguyen, C. T. C. High-*Q* UHF micromechanical radial-contour mode disk resonators. *J. Microelectromechan. Syst.* **14,** 1298–1310 (2005).
20. Favero, I. & Karrai, K. Optomechanics of deformable optical cavities. *Nature Photon.* **3,** 201–205 (2009).
21. Aspelmeyer, M., Kippenberg, T. J. & Marquardt, F. Cavity optomechanics. *Rev. Mod. Phys.* **86,** 1391–1452 (2014).
22. Baker, C. *et al.* Photoelastic coupling in gallium arsenide optomechanical disk resonators. *Opt. Express* **22,** 14072–14086 (2014).
23. Ding, L. *et al.* Wavelength-sized GaAs optomechanical resonators with gigahertz frequency. *Appl. Phys. Lett.* **98,** 113108 (2011).
24. Nguyen, D. T. *et al.* Ultrahigh *Q*-frequency product for optomechanical disk resonators with a mechanical shield. *Appl. Phys. Lett.* **103,** 241112 (2013).
25. Nguyen, D. T. *et al.* Improved optomechanical disk resonator sitting on a pedestal mechanical shield. *New J. Phys.* **17,** 023016 (2015).
26. Baker, C. *et al.* Critical optical coupling between a GaAs disk and a nanowaveguide suspended on the chip. *Appl. Phys. Lett.* **99,** 151117 (2011).
27. Parrain, D. *et al.* Damping of optomechanical disks resonators vibrating in air. *Appl. Phys. Lett.* **100,** 242105 (2012).
28. Love, A. E. H. *A Treatise on the Mathematical Theory of Elasticity* (Cambridge Univ. Press, 1906).

29. Onoe, M. Contour vibrations of isotropic circular plates. *J. Acoust. Soc. Am.* **28,** 1158–1162 (1956).
30. Hosaka, H., Itao, K. & Kuroda, S. Damping characteristics of beam-shaped micro-oscillators. *Sens. Actuators A* **49,** 87–95 (1995).
31. Oestreicher, H. L. Field and impedance of an oscillating sphere in a viscoelastic medium with an application to biophysics. *J. Acoust. Soc. Am.* **23,** 707–714 (1951).
32. Ekinci, K. L., Yang, Y. T. & Roukes, M. L. Ultimate limits to inertial mass sensing based upon nanoelectromechanical systems. *J. Appl. Phys.* **95,** 2682–2689 (2004).
33. Cleland, A. N. & Roukes, M. L. Noise processes in nanomechanical resonators. *J. Appl. Phys.* **92,** 2758–2769 (2002).
34. Zhu, H. & Lee, J. E. Y. Reversed nonlinear oscillations in lame-mode single-crystal-silicon microresonators. *IEEE Electron Device Lett.* **33,** 1492–1494 (2012).
35. Kaajakari, V., Mattila, T., Oja, A. & Seppa, H. Nonlinear limits for single-crystal silicon microresonators. *J. Microelectromech. Syst.* **13,** 715–724 (2004).
36. Philip, J. & Breazeale, M. A. Third-order elastic-constants and Grüneisen parameters of silicon and germanium between 3 and 300 °K. *J. Appl. Phys.* **54,** 752–757 (1983).
37. Olcum, S. *et al.* Weighing nanoparticles in solution at the attogram scale. *Proc. Natl Acad. Sci. USA* **111,** 1310–1315 (2014).
38. Millero, F. J. High precision magnetic float densimeter. *Rev. Sci. Instrum.* **38,** 1441–1444 (1967).
39. Taylor, M. A. *et al.* Subdiffraction-limited quantum imaging within a living cell. *Phys. Rev. X* **4,** 0011017 (2014).

Acknowledgements

E.G. and D.T.N. acknowledge support from the Research in Paris programme of the Ville de Paris and by the French National Research Agency through the NOMADE Project. E.G., C.B., W.H. and I.F. acknowledge support from the European Research Council through the GANOMS Project.

Author contributions

E.G. and I.F. conceived and designed the experiments, and developed the models. C.B., D.T.N. and W.H. contributed to the fabrication and experimental techniques. C.G. and A.L. grew the epitaxial material. E.G. performed the systematic experiments. All the authors discussed the results and wrote the paper.

Additional information

Supplementary information is available in the online version of the paper. Reprints and permissions information is available online at www.nature.com/reprints. Correspondence and requests for materials should be addressed to I.F.

Competing financial interests

The authors declare no competing financial interests.

Methods

Experiments. Light from an external tunable cavity diode laser is fibre-guided, polarization-controlled, injected into the chip's waveguide using a microlensed fibre, collected at the guide's output with a microscope objective and sent to a photodiode. The laser wavelength is first swept to acquire the optical spectrum of the disk and then set on the blue flank of a WGM resonance. In this configuration the mechanical information is imprinted onto the radiofrequency spectrum of light and revealed by a spectrum analyser plugged at the photodiode output.

Nanofabrication. The disks are fabricated out of a GaAs (320 nm)/$Al_{0.8}Ga_{0.2}As$ (2.000 nm)/GaAs wafer grown by molecular beam epitaxy. Disks are positioned in the vicinity of GaAs-tapered suspended waveguides to allow evanescent optical coupling. Disks and waveguides are patterned in a resist mask by electron-beam lithography and dry etched by inductively coupled plasma reactive ion etching with a mixture of $SiCl_4$ and Ar plasmas. The AlGaAs sacrificial layer is selectively underetched by HF to form the selected pedestals. A diluted HF:H_2O solution (1.22% in volume) at 4 °C is combined with a slow agitation in the solution to reach a pedestal radius below 200 nm.

Liquids. The three liquids employed in the experiments are inert non-ionic perfluorinated solutions from Galden (HT 170, HT 230 and HT 270).